Original Article

Improving the registration stability of cone-beam computed tomography with the Sphere-Mask Optical Positioning System: a feasibility study

Yan Zhang[1]^, Han Zhou[1], Yanan Jiang[1], Chuanfeng Wu[2], Yun Ge[1], Guoping Shan[1,4], Kaiyue Chu[3], Jundong Zhou[2], Jing Cai[3], Jianhua Jin[3], Ying Chen[1], Xiaolin Huang[1]

[1]School of Electronic Science and Engineering, Nanjing University, Nanjing, China; [2]Department of Radiotherapy, Suzhou Municipal Hospital, Suzhou, China; [3]Department of Radiotherapy, Nantong Tumor Hospital, Nantong, China; [4]Department of Radiation Physics, Zhejiang Cancer Hospital, Hangzhou, China

Contributions: (I) Conception and design: Y Zhang, Y Ge; (II) Administrative support: Y Ge, K Chu; (III) Provision of study materials or patients: C Wu, K Chu, J Zhou, J Cai, J Jin; (IV) Collection and assembly of data: Y Zhang, Y Jiang, Y Ge; (V) Data analysis and interpretation: Y Zhang, H Zhou, C Wu, Y Ge, K Chu, J Zhou, J Cai, J Jin; (VI) Manuscript writing: All authors; (VII) Final approval of manuscript: All authors.

Correspondence to: Yun Ge. School of Electronic Science and Engineering, Nanjing University, No. 163 Xianlin Avenue, Qixia District, Nanjing 210023, China. Email: geyun@nju.edu.cn; Kaiyue Chu. Department of Radiotherapy, Nantong Tumor Hospital, No. 30 Tongyang North Road, Pingchao Town, Tongzhou District, Nantong 226300, China. Email: chu_ky@163.com.

Background: Cone-beam computed tomography (CBCT) is an important tool for patient positioning in radiotherapy due to its outstanding advantages. However, the CBCT registration shows errors due to the limitations of the automatic registration algorithm and the nonuniqueness of manual verification results. The purpose of this study was to verify the feasibility of using the Sphere-Mask Optical Positioning System (S-M_OPS) to improve the registration stability of CBCT through clinical trials.

Methods: From November 2021 to February 2022, 28 patients who received intensity-modulated radiotherapy and site verification with CBCT were included in this study. S-M_OPS was used as an independent third-party system to supervise the CBCT registration result in real time. The supervision error was calculated based on the CBCT registration result and using the S-M_OPS registration result as the standard. For the head and neck, patients with a supervision error ≥3 or ≤–3 mm in 1 direction were selected. For the thorax, abdomen, pelvis, or other body parts, patients with a supervision error ≥5 or ≤–5 mm in 1 direction were selected. Then, re-registration was performed for all patients (selected and unselected). The registration errors of CBCT and S-M_OPS were calculated based on the re-registration results as the standard.

Results: For selected patients with large supervision errors, CBCT registration errors (mean ± standard deviation) in the latitudinal (LAT; left/right), vertical (VRT; superior/inferior), and longitudinal (LNG; anterior/posterior) directions were 0.90±3.20, –1.70±0.98, and 7.30±2.14 mm, respectively. The S-M_OPS registration errors were 0.40±0.14, 0.32±0.66, and 0.24±1.12 mm in the LAT, VRT, and LNG directions, respectively. For all patients, CBCT registration errors in the LAT, VRT, and LNG directions were 0.39±2.69, –0.82±1.47, and 2.39±2.93 mm, respectively. The S-M_OPS registration errors were –0.25±1.33, 0.55±1.27, and 0.36±1.34 mm for all patients in the LAT, VRT, and LNG directions, respectively.

^ ORCID: 0000-0003-2102-1823.

Conclusions: This study shows that S-M_OPS registration offers comparable accuracy to CBCT for daily registration. S-M_OPS, as an independent third-party tool, can prevent large errors in CBCT registration, thereby improving the accuracy and stability of CBCT registration.

Keywords: Cone-beam computed tomography (CBCT); Sphere-Mask Optical Positioning System (S-M_OPS); registration; stability

Submitted Sep 20, 2022. Accepted for publication Mar 03, 2023. Published online Mar 20, 2023.
doi: 10.21037/qims-22-989
View this article at: https://dx.doi.org/10.21037/qims-22-989

Introduction

The purpose of most image-guided positioning methods is to register the computed tomography (CT) image to calculate the tumor center position of a patient in the on-site coordinate system and move that information to the machine treatment isocenter. The accuracy of the registration determines the accuracy of the positioning.

Over the past decades, cone-beam computed tomography (CBCT) has become the standard for positioning in conventional fractionated and hypofractionated radiotherapy due to its outstanding advantages, including stereo imaging, sufficient contrast, and a low radiation dose (1,2). The registration methods used in CBCT-based positioning can mainly be divided into grayscale-based automatic registration methods (3-5), bony-based automatic registration methods (3,6-8), and manual registration methods (3,9). The accuracy of registration has been improved by the proposal of new registration algorithms. For example, XVI (Elekta Synergy, Stockholm, Sweden) uses a dual-image registration method that combines the grayscale and bony marker methods (10). Deng *et al.* (11) applied a combination of stationary wavelet transform and mutual information to compensate for the lack of spatial information in grayscale-based registration. In addition, there are many other registration methods, such as gradient-based methods (12,13) and deep learning–based registration methods (14-16). For example, Fu *et al.* (17) proposed a deformable registration method using biomechanically constrained deep learning networks. However, considering the limitations of the technology (14,18) and the imaging problems (e.g., scattering, artifacts) of CBCT (19-21), it is difficult to achieve high accuracy and stability for CBCT registration. Therefore, Al-Saleh *et al.* (22), in their review analyzing magnetic resonance imaging (MRI)-CT/CBCT registration, suggested using third-party tools independent of CBCT to measure registration accuracy. However, thus far, few tools can be used to supervise the registration accuracy of CBCT besides surface-guided radiation therapy (SGRT) techniques represented by Catalyst and Sentinel systems (23-26). However, these SGRT technologies cannot effectively supervise CBCT registration due to their poor accuracy (25). Therefore, radiation therapists usually use other techniques to aid CBCT registration clinically. For example, using gold fiducial markers improves the positioning accuracy for prostate cancer (27-29), and surgical clips help to localize the excision cavity for breast cancer (30-32). These auxiliary technologies are also affected by the imaging quality of CBCT. However, a recent study showed that Sphere-Mask Optical Positioning System (S-M_OPS) was not affected by imaging quality and provided comparable localization accuracy to CBCT. Hence, it could supervise CBCT-guided registration accuracy (33).

The purpose of this study was to use S-M_OPS as an independent third-party tool to supervise the process of CBCT registration, improve the accuracy and stability of CBCT registration, and verify the feasibility of the method through clinical trials.

Methods

S-M_OPS

S-M_OPS, developed by Nanjing University and the Nanjing Zhiyun Medical Device Research Institute, is a stereo infrared optical tracking system that can perform noninvasive, submillimeter-level localization and real-time tracking during positioning and treatment (34,35). The registration time required for S-M_OPS is 0.1 s (10 fps), which is much lower than that required by commonly used registration algorithms (65 s) and manual registration (82 s) (10). It is especially suitable for countries with a low amount of radiotherapy equipment per million population,

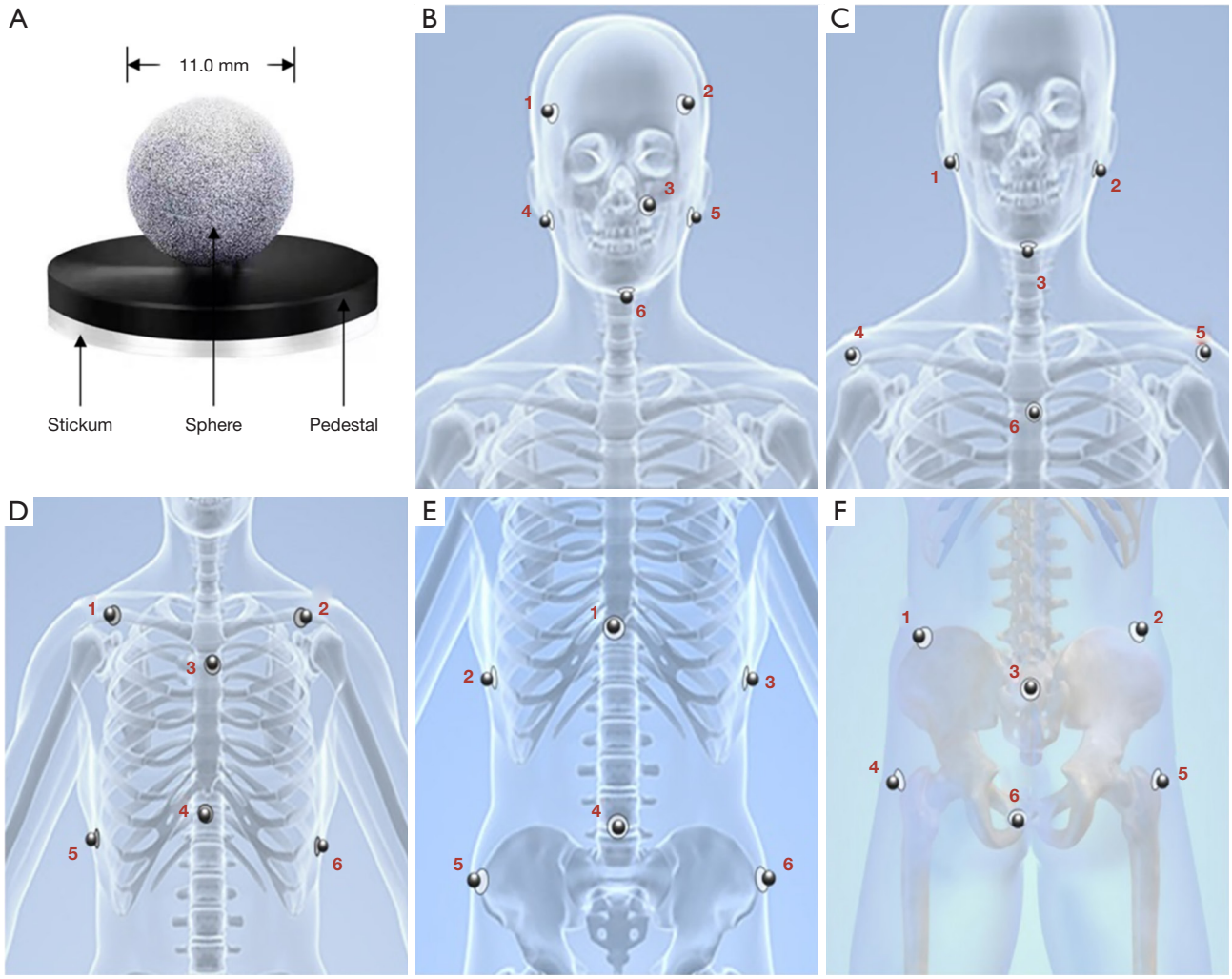

Figure 1 A schematic diagram of the infrared positioning sphere and the standardized placement of spheres in different parts. (A) Infrared positioning sphere. (B) The standardized placement of spheres in the head. (C) The standardized placement of spheres in the neck. (D) The standardized placement of spheres in the thorax. (E) The standardized placement of spheres in the abdomen. (F) The standardized placement of spheres in the pelvis (6 positioning spheres of each part on the thermoplastic mask are fixed to the bony markers).

such as low- and middle-income countries (36,37), due to its short registration time. S-M_OPS adopts point registration, which is a type of rigid registration (22). After 7 years of clinical trials [2016–2022], S-M_OPS has been demonstrated to be accurate and reliable (33).

S-M_OPS is composed of a binocular infrared camera, infrared positioning spheres, a thermoplastic mask, and the S-M_OPS treatment planning system. The positioning accuracy of the binocular infrared camera is 0.25 mm in three-dimensional (3D) space, and the diameter of the positioning sphere is 11 mm (*Figure 1*). During patient positioning, the positioning spheres are permanently fixed on the thermoplastic mask, which keeps the spheres and the thermoplastic mask from slipping during all fractions. When positioning and radiotherapy are conducted, S-M_OPS monitors the patient's position, posture, and breathing by tracking the positioning spheres on the thermoplastic mask during fractions in real time. S-M_OPS is compatible with most of the existing radiotherapy plans (especially the fractionated treatment with the thermoplastic mask), as it can apply the combination of positioning spheres and the thermoplastic mask to the whole body (including the head, neck, thorax, abdomen, and pelvis). By using the more sensitive thermoplastic mask and normalizing the position

of the positioning spheres (as shown in *Figure 1*), it is possible to capture patient activity with more sensitivity.

Patient selection and fixtures

A total of 28 patients who received intensity-modulate radiotherapy (IMRT) and site verification by CBCT were selected for this study. The distribution of sites examined was as follows: 1 case in the head and neck, 14 cases in the esophagus, 6 cases in the thorax, 2 cases in the abdomen, 3 cases in the pelvis, and 2 cases in other parts. The mean age of the patients was 68.4 years old, and the median age was 70 years (range, 52–85 years). The patient whose head and neck were scanned was immobilized with the thermoplastic mask. Patients whose thorax, abdomen, pelvis, and other parts were scanned were immobilized with the thermoplastic film and a vacuum.

After the patient was immobilized, the radiotherapists fixed the positioning spheres at the bony markers on the thermoplastic mask (as shown in *Figure 1*). The positions of the positioning spheres needed to reflect the body surface characteristics of the region of interest.

The study was conducted in accordance with the Declaration of Helsinki (as revised in 2013) and was approved by the Nantong Cancer Hospital, Medical Department, Medical Technology Access Management Committee. Informed consent was obtained from all the patients.

Image-guided protocol and trial procedure

The principle of positioning is moving the tumor center to the machine treatment isocenter within the tolerance of the error. Before the trial, radiotherapists fixed the positioning spheres on the linear accelerator and the couch. By rotating the accelerator and moving the couch, S-M_OPS could acquire the machine treatment isocenter of the linear accelerator by tracking the positioning spheres. In order to reduce the uncertainty generated by mechanical error, we carried out these steps before every fraction to obtain the correct machine treatment isocenter.

The detailed trial procedures are shown in *Figure 2* and described below.

The planning phase

Each patient was placed in the supine position and underwent CT scanning for planning. For the head and neck, the patient was scanned with a 3-mm slice thickness with a Brilliance Big Bore CT Scanner (Philips, Amsterdam, Netherlands). For the thorax, abdomen, and pelvis, the slice thickness was 5 mm. The CT data were then transmitted to the Pinnacle treatment planning system (Philips), and the S-M_OPS treatment planning system. All patients' therapy plans were generated by the Philips Pinnacle system. We obtained the position of the real tumor center (denoted as the real tumor center T_0, as shown in *Figure 3*) from the therapy plan. S-M_OPS delineated the positions of the spheres and calculated the associated parameters, which was the relative 3D spatial relationship between spheres and the tumor, denoted as the sphere-tumor relative relationship.

The registration phase

All patients underwent CBCT image acquisition with the XVI system (Elekta, Stockholm, Sweden). The XVI system is a CBCT unit integrated into the Synergy linear accelerator (Elekta, Stockholm, Sweden). The system consists of a kilovoltage-class X-ray source (producing 70- to 150-kVp diagnostic quality X-rays) and a flat panel detector (amorphous silicon/cesium iodide) mounted on 2 telescopic arms. In this clinical study, the field of view was set to the medium field of view, the collimator/filter was set to M20/F1, and the X-ray tube voltage was set to 120 kVp.

The XVI system automatically registered the collected CBCT data and obtained the location of the tumor center (denoted as CBCT tumor center T_1, as shown in *Figure 3*) (10). According to 3 components of T_1, radiotherapists determined the positioning errors in the latitudinal (LAT; left/right), vertical (VRT; superior/inferior), and longitudinal (LNG) directions and moved the couch. Meanwhile, S-M_OPS was used for independent third-party supervision. By tracking the position of the positioning spheres in real time and using the sphere–tumor relative relationship obtained in the previous phase, the S-M_OPS could calculate the position of the tumor center (denoted as S-M_OPS tumor center T_2, as shown in *Figure 3*) and the supervision result $\vec{D}_{Supervision}$ (the 3D vector from T_1 to T_2, the 3 components of which represented the registration errors in the LAT, LNG, and VRT directions).

The re-registration phase

The clinically accepted registration error cannot exceed ±3.0 mm for the head and neck in any direction and cannot exceed ±5.0 mm for the thorax, abdomen, pelvis, and other parts (38-40). Therefore, for the head and neck, we selected a patient whose registration error was ≥3 or ≤–3 mm in 1 direction in the supervision result. For the thorax,

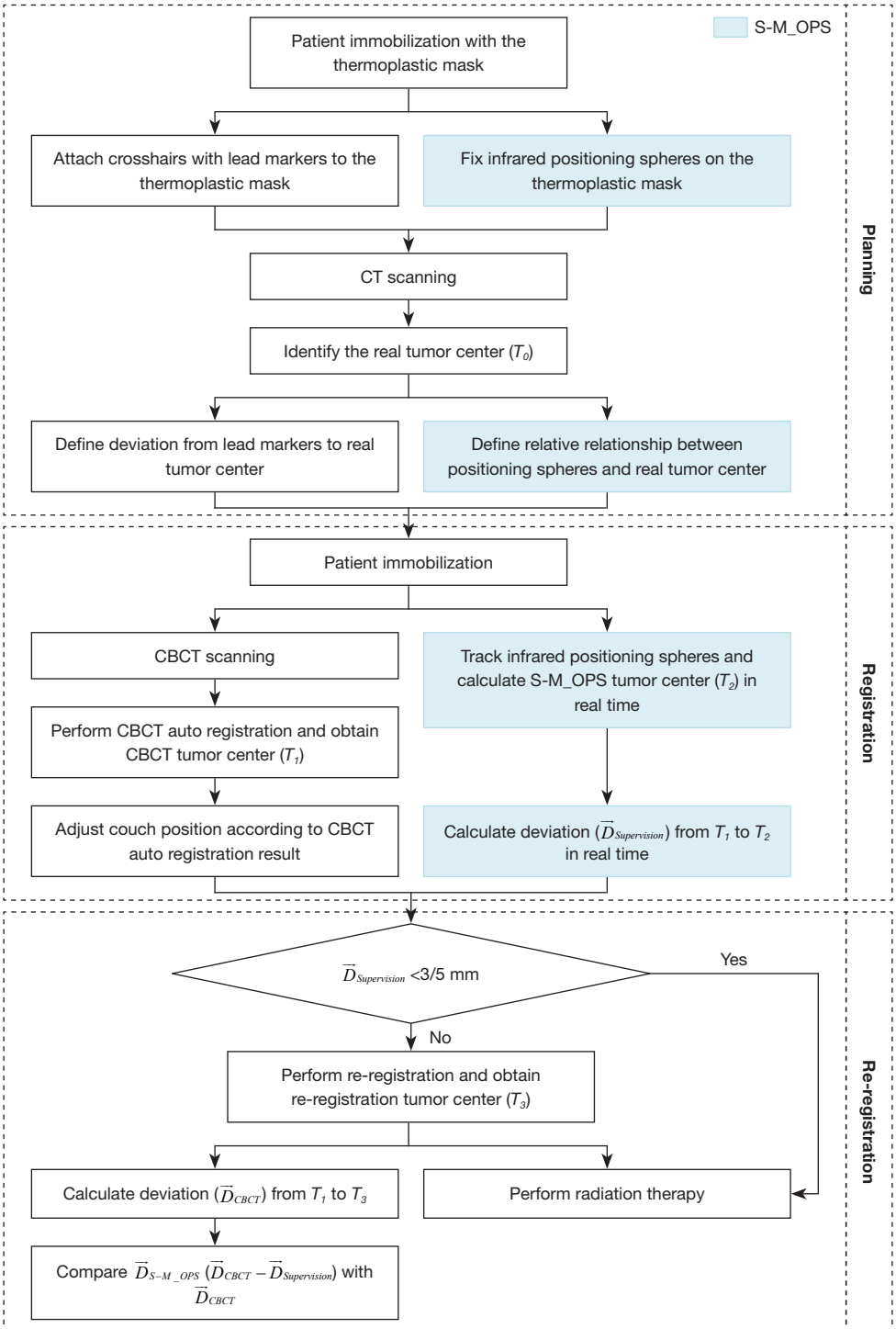

Figure 2 The flowchart of the clinical trial for coregistration of CBCT and S-M_OPS. The upper part shows the planning phase. The middle part shows the registration phase. The lower part shows the re-registration phase. CBCT, cone-beam computed tomography; S-M_OPS, Sphere-Mask Optical Positioning System.

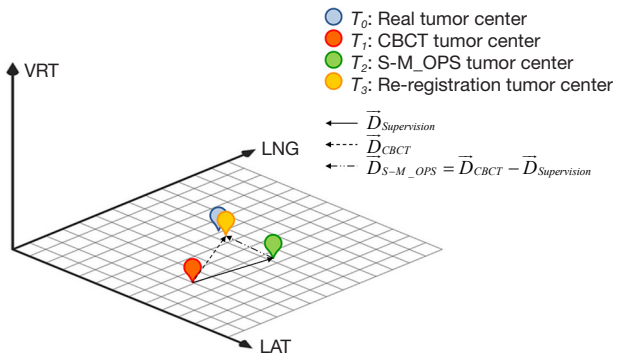

Figure 3 A schematic diagram of the 3-dimensional spatial relationship of tumor centers obtained by CBCT registration (T_1, red), S-M_OPS registration (T_2, green), and re-registration (T_3, yellow). CBCT, cone-beam computed tomography; LAT, latitudinal; LNG, longitudinal; VRT, vertical; S-M_OPS, Sphere-Mask Optical Positioning System.

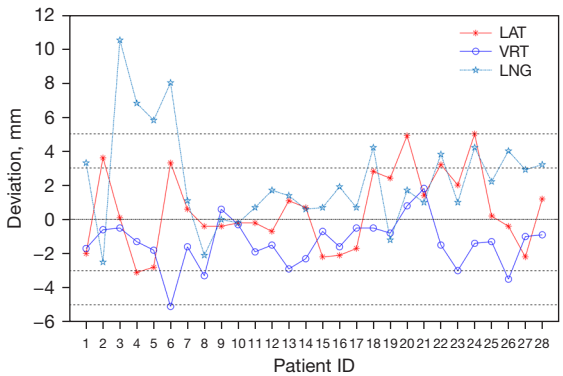

Figure 4 The errors distribution of CBCT registration in the LAT, LNG, and VRT directions of S-M_OPS recording. CBCT, cone-beam computed tomography; LAT, latitudinal; VRT, vertical; LNG, longitudinal; S-M_OPS, Sphere-Mask Optical Positioning System.

abdomen, pelvis, and other parts, we selected patients whose registration error was ≥5 or ≤–5 mm in 1 direction in the supervision result. Then, for the patients selected, we re-registered rigorously and obtained the re-registration result (denoted as re-registration tumor center T_3, as shown in *Figure 3*).

We viewed the position of the re-registration tumor center, T_3, as the position of the real tumor center, T_0, in the CBCT image and used the re-registration tumor center, T_3, as the standard to evaluate the accuracy of CBCT registration and S-M_OPS registration. Therefore, the registration error was equal to the deviation from the tumor center (T_1 or T_2) to the re-registration tumor center, T_3. We denoted the CBCT registration error as $\vec{D}_{CBCT}$ (the 3D vector from T_1 to T_3, of which the 3 components represented the registration errors in the LAT, LNG, and VRT directions, as shown in *Figure 3*). In addition, we denoted the S-M_OPS registration error as $\vec{D}_{S-M\_OPS}$ ($\vec{D}_{S-M\_OPS} = \vec{D}_{CBCT} - \vec{D}_{Supervision}$), the 3D vector from T_2 to T_3, of which the 3 components represented the registration errors in the LAT, LNG, and VRT directions, as shown in *Figure 3*).

Finally, based on the re-registration result, the radiotherapists moved the couch and used the Synergy linear accelerator to treat the patient.

Additional measures were taken to reduce some uncertainties. For example, we supervised the machine treatment isocenter to reduce the influence of mechanical error. However, other uncertainties could influence the registration accuracy during the conventional fraction, including imaging quality, human factors, and intrafraction motion. We included these uncertainties because these factors were unavoidable for CBCT registration.

Statistical analysis

For CBCT registration errors and S-M_OPS registration errors, the Mann-Whitney test was adopted to test for the equality of means, and the *F* test was applied to test for the equality of variances. Statistical significance was defined as $P<0.05$.

Results

The distribution of CBCT registration errors supervised by S-M_OPS in the LAT, LNG, and VRT directions (the 3 components of $\vec{D}_{Supervision}$) is shown in *Figure 4*. For all data, the mean errors in LAT, VRT, and LNG directions were 0.64, –1.37, and 2.04 mm, respectively. Among these data, we found that 5 groups of data did not meet the registration requirement clinically, including patient 3 (10.5 mm in the LNG direction), patient 4 (6.8 mm in the LNG direction), patient 5 (5.8 mm in the LNG direction), patient 6 (–5.1 mm in the VRT direction, 8.0 mm in the LNG direction), and patient 24 (5.0 mm in the LAT direction).

Patient 3's treatment position was in the lungs. We obtained the location of the real tumor center T_0 from the CT images for the radiation therapy plan and the location of the CBCT tumor center T_1 from the CBCT

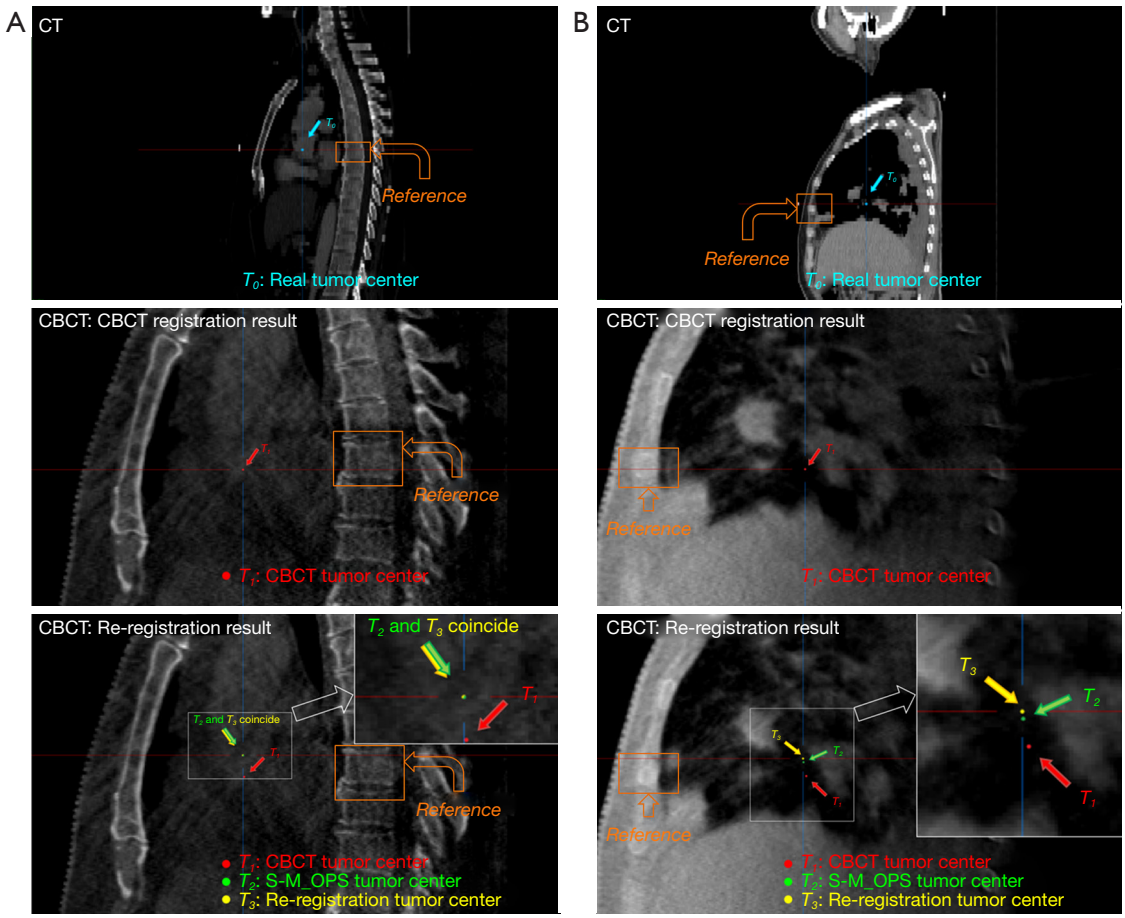

Figure 5 The registration results of CBCT, S-M_OPS, and re-registration. (A) The data on the sagittal plane of patient 3 (from top to bottom: CT image, CBCT image, and CBCT image). (B) The data on the sagittal plane of patient 4 (from top to bottom: CT image, CBCT image, and CBCT image). CBCT, cone-beam computed tomography; S-M_OPS, Sphere-Mask Optical Positioning System; CT, computed tomography.

images after registration. *Figure 5A* shows the CT image and CBCT images on the sagittal plane. We noticed that, with the vertebra as the reference, T_0 was located on the top of the reference vertebral body in the LNG direction in the CT image. However, the CBCT registration result showed that the CBCT tumor center T_1 was located at the bottom of the reference vertebral body, which meant there was a large deviation from the real tumor center, T_0, in the LNG direction. Taking the vertebral body and associated soft tissues as the reference marks, we re-registered and obtained the re-registration tumor center, T_3.

Patient 4's treatment position was also in the lungs. *Figure 5B* shows the CT image and CBCT images on the sagittal plane. Taking the rib as the reference, the real tumor center, T_0, was located above the reference rib in the LNG direction in the CT image. However, the CBCT registration result showed that the CBCT tumor center, T_1, passed through the middle of the rib, which meant there was an obvious deviation from the real tumor center, T_0, in the LNG direction. Taking the rib and associated soft tissues as the reference marks, we re-registered and obtained the re-registration tumor center, T_3.

Patient 5's treatment position was in the esophagus. *Figure 6A* shows the CT image and CBCT image on the sagittal plane. With the spine as the reference, the real tumor center, T_0, passed through the inferior plane of the reference spinous process in the LNG direction in the CT image. However, the CBCT registration result showed that the CBCT tumor center, T_1, passed through the top of the next spinous process, which meant there was

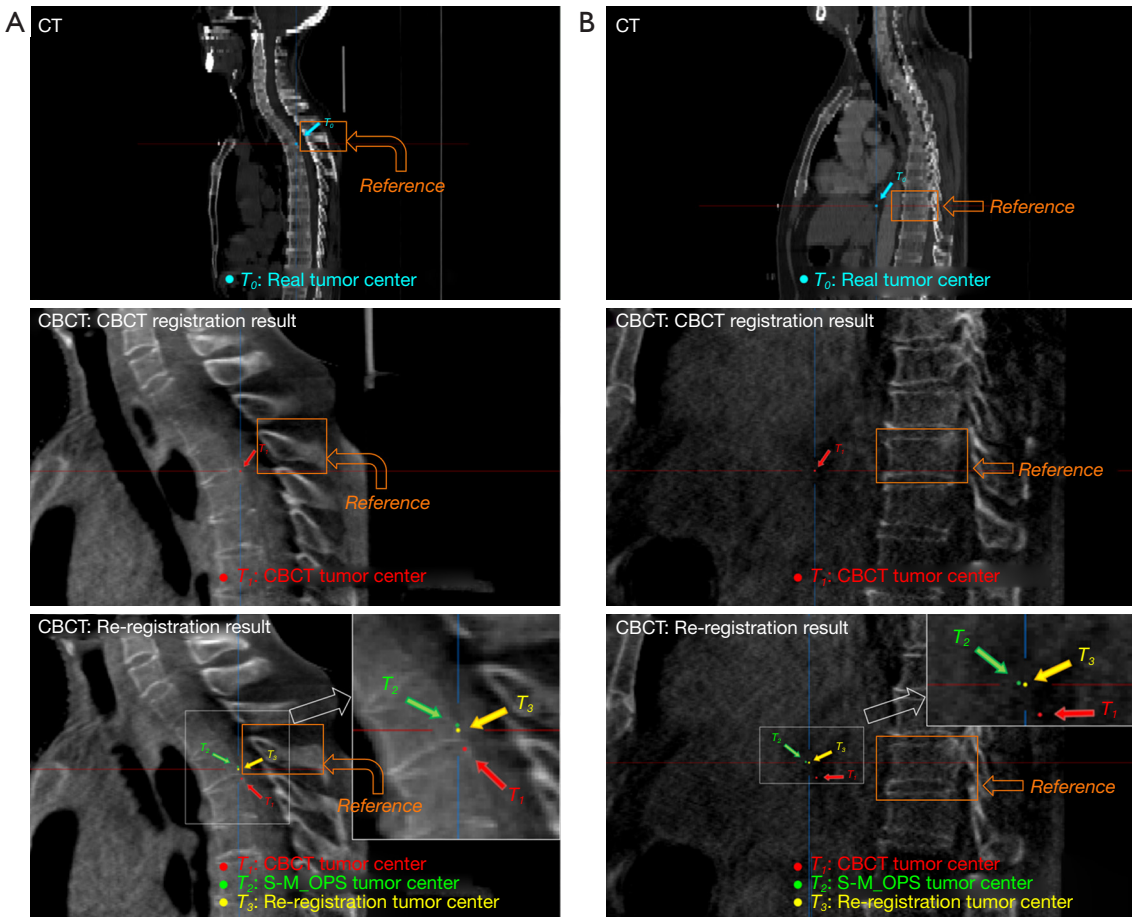

Figure 6 The registration results of CBCT, S-M_OPS, and re-registration. (A) The data on the sagittal plane of patient 5 (from top to bottom: CT image, CBCT image, and CBCT image). (B) The data on the sagittal plane of patient 6 (from top to bottom: CT image, CBCT image, and CBCT image). CBCT, cone-beam computed tomography; S-M_OPS, Sphere-Mask Optical Positioning System; CT, computed tomography.

a certain deviation from the real tumor center, T_0, in the LNG direction. Taking the spinous process and associated soft tissues as the reference marks, we re-registered and obtained the re-registration tumor center, T_3.

Patient 6's treatment position was in the bronchi and lungs. *Figure 6B* shows the CT image and CBCT images on the sagittal plane. Taking the vertebra as the reference, the real tumor center, T_0, passed through the middle of the vertebral body in the LNG direction in the CT image. However, the CBCT registration result showed that the CBCT tumor center, T_1, was located at the bottom of the vertebral body, which meant there was an obvious deviation from the real tumor center, T_0, in the LNG direction. Taking the vertebral body and associated soft tissues as the reference marks, we re-registered and obtained the re-registration tumor center, T_3.

Patient 24's treatment position was in the esophagus. *Figure* 7 shows the CT image and CBCT images on the transverse plane. In the CT image, with the spinous process as the reference, the real tumor center, T_0, lay to its left and intersected it. However, according to the CBCT registration results, the CBCT tumor center, T_1, was located on the left side of the vertebral body but did not intersect, which meant there was an obvious deviation from the real tumor center, T_0, in the LAT direction. Due to the nonnegligible deviation in the LNG direction (LNG =4.2 mm), there might have been an error in the selection of the optimal layer of CBCT for registration (the slice thickness of CBCT was 5 mm). Taking the spinous process and associated soft tissues as the reference marks, we adjusted the layer of CBCT data,

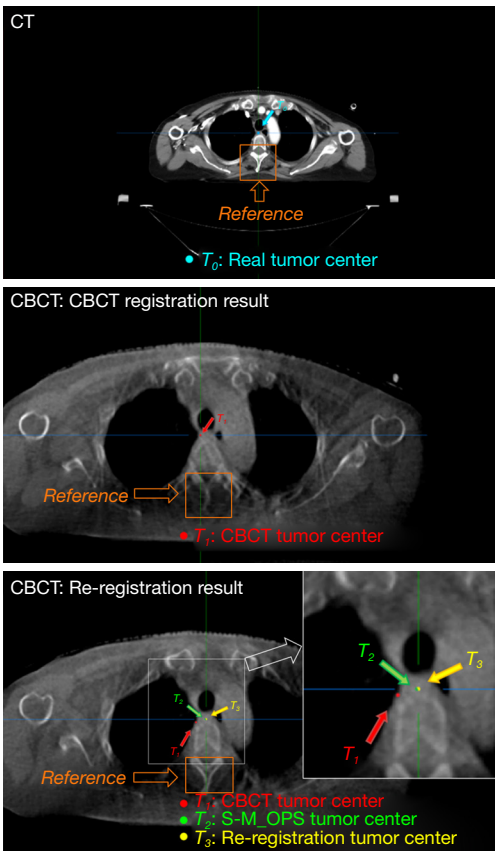

Figure 7 The registration results of CBCT, S-M_OPS, and re-registration. The data on the transverse plane of patient 24 (from top to bottom: CT image, CBCT image, and CBCT image). CBCT, cone-beam computed tomography; S-M_OPS, Sphere-Mask Optical Positioning System; CT, computed tomography.

re-registered it, and obtained the re-registration tumor center, T_3.

For each of the above 5 patients, we projected all points (including the CBCT tumor center, T_1, S-M_OPS tumor center, T_2, and re-registration tumor center, T_3) to the same CBCT image and calculated all errors (including CBCT registration error $\vec{D}_{CBCT}$ and S-M_OPS registration error $\vec{D}_{S-M\_OPS}$) based on these points. All the above results are shown in *Table 1*. When we compared the CBCT registration error (the 3 components of $\vec{D}_{CBCT}$) and the S-M_OPS registration error (the 3 components of $\vec{D}_{S-M\_OPS}$), as shown in *Figure 8*, we found that the absolute values of the 3 components of $\vec{D}_{S-M\_OPS}$ were all less than those of $\vec{D}_{CBCT}$. CBCT registration errors (mean ± standard deviation, denoted as mean ± SD) in the LAT, VRT, and LNG directions were 0.90±3.20, –1.70±0.98, and 7.30±2.14 mm, while S-M_OPS registration errors were 0.40±0.14, 0.32±0.66, and 0.24±1.12 mm, respectively.

In addition, for the remaining 23 patients, we also re-registered them. In all 28 patients (5 selected patients and the remaining 23 patients), CBCT registration errors (mean ± SD) in the LAT, VRT, and LNG directions are shown in *Table 2*. The results of the *t*-test and *F* test and their associated P values are shown in *Table 2*). Significant differences favoring S-M_OPS registration in all directions were observed (P<0.01 in the *t*-test or *F* test). As mentioned in section "Image-guided protocol and trial procedure", the generally accepted clinical registration error should be no more than ±3.0 mm in 1 direction for the head and neck, and no more than ±5.0 mm in 1 direction for the thorax, abdomen, and pelvis (38-40). Therefore, for the CBCT registration, 82.14% of patients (23/28) met the clinical requirements of registration. For S-M_OPS registration, 100% of the patients (28/28) met the clinical requirements of registration.

Discussion

In terms of accuracy, we found that in all patients, the absolute value of the means of S-M_OPS registration errors (–0.25, 0.55, and 0.36 mm) were all smaller than those of CBCT registration errors (0.39, –0.82, and 2.39 mm). In terms of stability, all (28/28) S-M_OPS registration results met the clinical registration requirement, while 85.71% (24/28) CBCT registrations met the clinical requirements. The SDs of the S-M_OPS registration errors (1.33, 1.27, and 1.34 mm) were smaller than those of the CBCT registration errors (2.69, 1.47, and 2.93 mm), which indicated that S-M_OPS could improve the feasibility of CBCT registration stability ($P<10^{-3}$ in the LAT direction; P=0.23 in the VRT direction; $P<10^{-4}$ in the LNG direction).

The causes of CBCT registration errors were complex. First, for all of the patients, the CBCT registration error in the LNG direction was the greatest. This was attributed to the existence of thickness (typically 3 or 5 mm) between layers of data acquired by planning CT (usually helical CT). Therefore, compared with those of the horizontal data, the reconstruction results of the LNG data were poor, which would affect the accuracy of CBCT registration (41,42). In addition, during manual verification, it was difficult for the radiation therapists to select the data with large errors in the LNG direction from the sagittal plane image or coronal plane image with poor reconstruction results. Second, the imaging quality of the CBCT (such as scattering and

Table 1 Registration results and registration errors for selected patients

Patient ID	CBCT registration result T_1 (mm)	S-M_OPS registration result T_2 (mm)	Re-registration result T_3 (mm)	CBCT registration error $\vec{D}_{CBCT}$ (mm)	S-M_OPS registration error $\vec{D}_{S-M\_OPS}$ (mm)
Patient 3	0, 0, 0	0.1, –0.5, 10.5	0.5, –0.5, 10.5	0.5, –0.5, 10.5	0.4, 0, 0
Patient 4	0, 0, 0	–3.1, –1.3, 6.8	–2.5, –1.5, 8.5	–2.5, –1.5, 8.5	0.6, –0.2, 1.7
Patient 5	0, 0, 0	–2.8, –1.8, 5.8	–2.5, –1.5, 4.5	–2.5, –1.5, 4.5	0.3, 0.3, –1.3
Patient 6	0, 0, 0	3.3, –5.1, 8	3.5, –3.5, 7.5	3.5, –3.5, 7.5	0.2, 1.6, –0.5
Patient 24	0, 0, 0	5, –1.4, 4.2	5.5, –1.5, 5.5	5.5, –1.5, 5.5	0.5, –0.1, 1.3

Values are shown in 3-dimensional coordinates or 3-dimensional vectors, with 3 components representing the registration results or registration errors in the LAT, LNG, and VRT directions, respectively. CBCT, cone-beam computed tomography; S-M_OPS, Sphere-Mask Optical Positioning System; LAT, latitudinal; VRT, vertical; LNG, longitudinal.

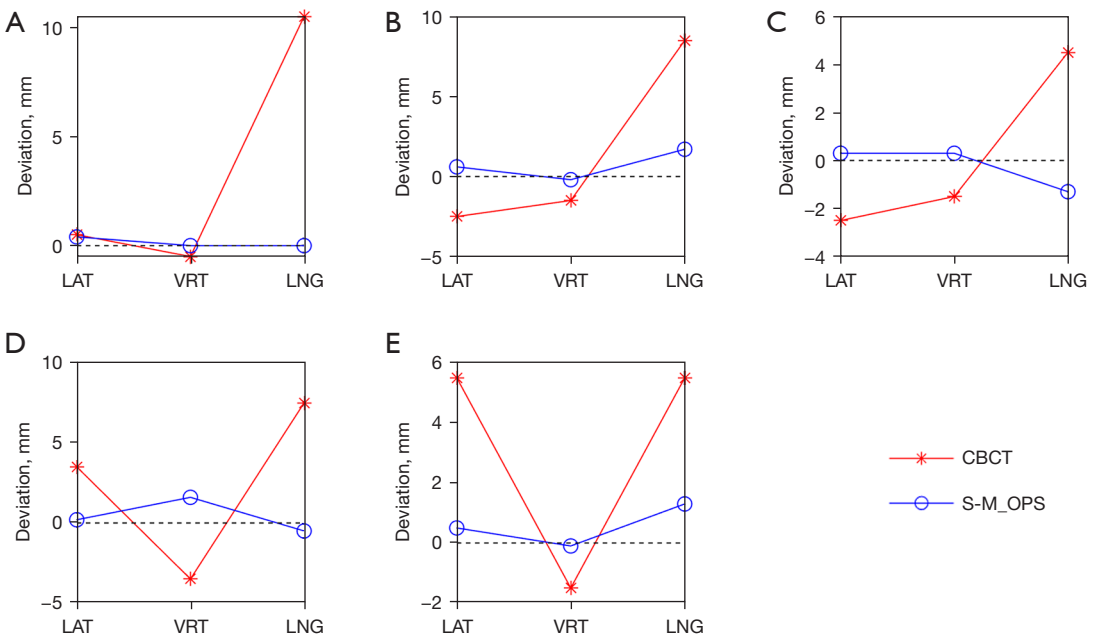

Figure 8 CBCT registration errors compared to S-M_OPS registration errors in the LAT, VRT, and LNG directions. (A) Patient 3. (B) Patient 4. (C) Patient 5. (D) Patient 6. (E) Patient 24. CBCT, cone-beam computed tomography; S-M_OPS, Sphere-Mask Optical Positioning System; LAT, latitudinal; LNG, longitudinal; VRT, vertical.

Table 2 Registration errors for all patients and results of statistical tests for differences between CBCT registration error and S-M_OPS registration error

Direction	CBCT registration error (mm)	S-M_OPS registration error (mm)	Difference	
			Mann-Whitney test	*F* test
LAT	0.39±2.69	–0.25±1.33	0.22	$<10^{-3}$
VRT	–0.82±1.47	0.55±1.27	$<10^{-3}$	0.23
LNG	2.39±2.93	0.36±1.34	$<10^{-2}$	$<10^{-4}$

Values are shown in mean ± SD or P value (Mann-Whitney test and *F* test). CBCT, cone-beam computed tomography; S-M_OPS, Sphere-Mask Optical Positioning System; LAT, latitudinal; VRT, vertical; LNG, longitudinal; SD, standard deviation.

artifacts) was also a factor that affected the registration results (19,20). For example, in the results of patient 4 (*Figure 5B*), it could be seen that the CBCT reconstructed image had low soft-tissue contrast, relatively large noise, and inconspicuous bony markers, which meant the CBCT imaging quality could not be improved by changing the window width and window level. Therefore, the result of grayscale-based registration or bony marker-based registration was poor, and the result of manual verification was also affected. Currently, the pursuits of a low acquisition time and low additional radiation (43-45) make it difficult to improve the quality of CBCT imaging. However, S-M_OPS adopts point registration, and the result is only related to the sphere–tumor relative relationship, which reduces the dependence on CT/CBCT imaging quality.

In addition to the above reasons related to CT/CBCT imaging, other uncertainties affected CBCT registration, which are discussed below.

The position of the real tumor center T_0

When designing the radiotherapy plan according to the intersection of the laser line projections on the thermoplastic mask, radiotherapists fix the lead marks on the thermoplastic mask. According to the lead markers imaged on the CT images, dosimetrists determine the real tumor center, T_0 (the intersection of lead markers on CT images). However, due to the existence of CT thickness, the lead markers fixed on the thermoplastic mask will appear on multiple consecutive slices, and the center of the lead mark is visually determined by the dosimetrists, which might result in the wrong tumor center, T_0', in the LNG direction in CT images. This phenomenon occurred in all 5 of the selected patients. Especially for patient 3 (*Figure 5A*), we found that the lead marker was displayed as a cylinder instead of the original spherical shape, which would affect the design of the radiotherapy plan or subsequent registration. To solve this problem, S-M_OPS is associated with the tumor center through the use of 6 positioning spheres attached to the thermoplastic mask. The diameters of the positioning spheres are 11.0 mm, which can also be imaged by the CT and appear in at least 2 slices. The S-M_OPS treatment planning system can detect the outline of the sphere in each slice automatically and calculate the sphere center based on the detected outlines. In other words, unlike the lead markers used in the traditional method, the S-M_OPS sphere center must not be determined on a specific CT slice.

Human factors

Uncertainties caused by human factors are unavoidable. Due to different experiences, different radiation therapists produce different registration results, including different manual registration results and different manual verification results after automatic registration. In addition, there are many other manual factors. For example, when designing the radiotherapy plan mentioned above, radiotherapists need to fix the lead marks on the thermoplastic mask. However, there might be deviations when fixing lead marks due to human subjectivity. For example, in patient 24 (*Figure 7*), we found that the left lead marker and the right lead mark were not on the same horizontal line (the LAT direction), which could lead to the error in determining the real tumor center, T_0. However, immobilizing positioning spheres does not require high precision because the S-M_OPS treatment planning system can recognize the positions of positioning spheres automatically, which reduces the impact of human factors on registration accuracy.

Intrafraction motion

Intrafraction motion, which is caused by the respiratory system, musculoskeletal system, cardiac system, and gastrointestinal system, has been an increasingly important issue in the era of image-guided radiotherapy (46). For example, considering the XVI system performed a 360° rotation in 2 min (660 projections) or a 200° rotation in 4 min (1,320 projections) in this study, the intrafraction motion was unavoidable, and intrafraction motion would lead to uncertainty in the CBCT registration. However, S-M_OPS registration did not require the time to conduct the imaging. Instead, it needed only about 0.1 s to register. As a result, S-M_OPS could reduce the uncertainty caused by intrafraction motion.

Other factors

In addition, mechanical errors and the specificity of different CBCT automatic registration algorithms are also uncertainties that affect the accuracy of CBCT registration.

Finally, we compared different techniques' registration accuracy (24,26,47,48), as shown in *Table 3*. In general, the registration accuracy and stability of S-M_OPS were much better than those of the Sentinel system, Catalyst system, and surgical clips, and S-M_OPS could provide comparable positioning accuracy to a gold fiducial. However, the gold

Table 3 Registration errors of different technologies

Technologies	LAT (mm)	VRT (mm)	LNG (mm)
S-M_OPS (cancer in the head and neck, thorax, and pelvis)	–0.25±1.33	0.55±1.27	0.36±1.34
Surgical clips (breast cancer, cup A–B, supine cohort)	2.6±3.3	2.3±3.2	1.8±3.2
Gold fiducial (prostate cancer)	0.54±2.20	0.70±2.20	0.90±2.30
Sentinel (cancer in the head and neck, thorax, and pelvis)	–1.0±3.7	1.1±6.4	–1.8±6.0
Catalyst (cancer in the head and neck, thorax, and pelvis)	0.7±2.8	–1.3±4.0	1.5±3.6

Values are shown in mean ± SD. S-M_OPS, Sphere-Mask Optical Positioning System; LAT, latitudinal; VRT, vertical; LNG, longitudinal; SD, standard deviation.

fiducial needs to be implanted into the tumor to assist in positioning. Doing so requires multiple scans and requires calibration prior to each scan, which involves additional radiation and additional time. For the surgical clip, its registration accuracy depends on the surgeon's surgical technique and the number of clips inserted (30). The Sentinel and Catalyst systems use structured light to capture the 3D surface of the patient and register the acquired surface to the previously recorded one for positioning error detection. However, surface-based registration has several drawbacks. First, the thorax and pelvic surfaces present symmetric shapes along the VRT direction, adversely affecting the positioning accuracy in the LNG and VRT direction (49). Second, the surface is prone to deformation due to the level of organ filling or loss of weight, and the surfaces of overweight patients are hard to reproduce. In light of these factors, surface-based registration accuracy is limited.

Conclusions

This study verified the feasibility of S-M_OPS to improve the registration stability of CBCT and proposed a new solution to improving registration accuracy and stability. The solution was to use S-M_OPS as an independent third-party system together with other registration methods. This method was not only suitable for CBCT but also for multimodal image acquisition methods, including MRI and ultrasound imaging.

Acknowledgments

Funding: This work was supported by the Jiangsu Provincial Social Development Key R&D Program (grant No. BE2020685).

Footnote

Conflicts of Interest: All authors have completed the ICMJE uniform disclosure form (available at https://qims.amegroups.com/article/view/10.21037/qims-22-989/coif). The authors have no conflicts of interest to declare.

Ethical Statement: The authors are accountable for all aspects of the work in ensuring that questions related to the accuracy or integrity of any part of the work are appropriately investigated and resolved. This study was conducted in accordance with the Declaration of Helsinki (as revised in 2013). The study was approved by the Nantong Cancer Hospital, Medical Department, Medical Technology Access Management Committee, and informed consent was obtained from all the patients.

References

1. Sarkar B, Munshi A, Ganesh T, Manikandan A, Krishnankutty S, Chitral L, Pradhan A, Kalyan Mohanti B. Technical Note: Rotational positional error corrected intrafraction set-up margins in stereotactic radiotherapy: A spatial assessment for coplanar and noncoplanar geometry. Med Phys 2019;46:4749-54.
2. Bissonnette JP, Balter PA, Dong L, Langen KM, Lovelock

DM, Miften M, Moseley DJ, Pouliot J, Sonke JJ, Yoo S. Quality assurance for image-guided radiation therapy utilizing CT-based technologies: a report of the AAPM TG-179. Med Phys 2012;39:1946-63.
3. Ai XQ, Tang CQ, Wu H, Garbo T, Wang X, Liu JP, Cao YF, Jin H. Comparison of positioning accuracy of different registration methods and dosimetric analysis of adaptive radiotherapy for breast cancer after breast conserving surgery. Transl Cancer Res 2020;9:3274-81.
4. Friedli L, Kloukos D, Kanavakis G, Halazonetis D, Gkantidis N. The effect of threshold level on bone segmentation of cranial base structures from CT and CBCT images. Sci Rep 2020;10:7361.
5. Sharp GC, Kandasamy N, Singh H, Folkert M. GPU-based streaming architectures for fast cone-beam CT image reconstruction and demons deformable registration. Phys Med Biol 2007;52:5771-83.
6. Schmidt RM, Delgadillo R, Ford JC, Padgett KR, Studenski M, Abramowitz MC, Spieler B, Xu Y, Yang F, Dogan N. Assessment of CT to CBCT contour mapping for radiomic feature analysis in prostate cancer. Sci Rep 2021;11:22737.
7. Machiels M, Jin P, van Gurp CH, van Hooft JE, Alderliesten T, Hulshof MCCM. Comparison of carina-based versus bony anatomy-based registration for setup verification in esophageal cancer radiotherapy. Radiat Oncol 2018;13:48.
8. Thomas M, De Roover R, van der Merwe S, Lambrecht M, Defraene G, Haustermans K. The use of tumour markers in oesophageal cancer to quantify setup errors and baseline shifts during treatment. Clin Transl Radiat Oncol 2020;26:8-14.
9. Veiga C, McClelland J, Moinuddin S, Lourenço A, Ricketts K, Annkah J, Modat M, Ourselin S, D'Souza D, Royle G. Toward adaptive radiotherapy for head and neck patients: Feasibility study on using CT-to-CBCT deformable registration for "dose of the day" calculations. Med Phys 2014;41:031703.
10. Campbell A, Owen R, Brown E, Pryor D, Bernard A, Lehman M. Evaluating the accuracy of the XVI dual registration tool compared with manual soft tissue matching to localise tumour volumes for post-prostatectomy patients receiving radiotherapy. J Med Imaging Radiat Oncol 2015;59:527-34.
11. Deng JM, Yue HZ, Zhuo ZZ, Yan HG, Liu D, Li HY. A stationary wavelet transform based approach to registration of planning CT and setup cone beam-CT images in radiotherapy. J Med Syst 2014;38:40.
12. Yu G, Liang Y, Yang G, Shu H, Li B, Yin Y, Li D. Accelerated gradient-based free form deformable registration for online adaptive radiotherapy. Phys Med Biol 2015;60:2765-83.
13. Markelj P, Tomaževič D, Likar B, Pernuš F. A review of 3D/2D registration methods for image-guided interventions. Med Image Anal 2012;16:642-61.
14. Xiao H, Teng X, Liu C, Li T, Ren G, Yang R, Shen D, Cai J. A review of deep learning-based three-dimensional medical image registration methods. Quant Imaging Med Surg 2021;11:4895-916.
15. Teng X, Chen Y, Zhang Y, Ren L. Respiratory deformation registration in 4D-CT/cone beam CT using deep learning. Quant Imaging Med Surg 2021;11:737-48.
16. Hu R, Yan H, Nian F, Mao R, Li T. Unsupervised computed tomography and cone-beam computed tomography image registration using a dual attention network. Quant Imaging Med Surg 2022;12:3705-16.
17. Fu Y, Wang T, Lei Y, Patel P, Jani AB, Curran WJ, Liu T, Yang X. Deformable MR-CBCT prostate registration using biomechanically constrained deep learning networks. Med Phys 2021;48:253-63.
18. Pluim JPW, Muenzing SEA, Eppenhof KAJ, Murphy K. The truth is hard to make: Validation of medical image registration. 2016 23rd International Conference on Pattern Recognition (ICPR); 04-08 December 2016; Cancun, Mexico; IEEE, 2016:2294-300.
19. Graham SA, Moseley DJ, Siewerdsen JH, Jaffray DA. Compensators for dose and scatter management in cone-beam computed tomography. Med Phys 2007;34:2691-703.
20. Boda-Heggemann J, Lohr F, Wenz F, Flentje M, Guckenberger M. kV cone-beam CT-based IGRT: a clinical review. Strahlenther Onkol 2011;187:284-91.
21. Lei Y, Wang T, Tian S, Dong X, Jani AB, Schuster D, Curran WJ, Patel P, Liu T, Yang X. Male pelvic multi-organ segmentation aided by CBCT-based synthetic MRI. Phys Med Biol 2020;65:035013.
22. Al-Saleh MA, Alsufyani NA, Saltaji H, Jaremko JL, Major PW. MRI and CBCT image registration of temporomandibular joint: a systematic review. J Otolaryngol Head Neck Surg 2016;45:30.
23. Al-Hallaq HA, Cerviño L, Gutierrez AN, Havnen-Smith A, Higgins SA, Kügele M, Padilla L, Pawlicki T, Remmes N, Smith K, Tang X, Tomé WA. AAPM task group report 302: Surface-guided radiotherapy. Med Phys 2022;49:e82-e112.
24. Stieler F, Wenz F, Scherrer D, Bernhardt M, Lohr F.

Clinical evaluation of a commercial surface-imaging system for patient positioning in radiotherapy. Strahlenther Onkol 2012;188:1080-4.
25. Kadman B, Takemura A, Ito T, Okada N, Kojima H, Ueda S. Accuracy of patient setup positioning using surface-guided radiotherapy with deformable registration in cases of surface deformation. J Appl Clin Med Phys 2022;23:e13493.
26. Stieler F, Wenz F, Shi M, Lohr F. A novel surface imaging system for patient positioning and surveillance during radiotherapy. A phantom study and clinical evaluation. Strahlenther Onkol 2013;189:938-44.
27. Jmour O, Benna M, Champagnol P, Ben Mrad M, Hamrouni A, Obeid L, Lahmamssi C, Bousarsar A, Vial N, Rehailia-Blanchard A, Sotton S, Lan M, Langrand-Escure J, Vallard A, Magné N. CBCT evaluation of inter- and intra-fraction motions during prostate stereotactic body radiotherapy: a technical note. Radiat Oncol 2020;15:85.
28. Nolan CP, Forde EJ. A review of the use of fiducial markers for image-guided bladder radiotherapy. Acta Oncol 2016;55:533-8.
29. DE Cicco L, Marzoli L, Lorusso R, Mancuso RM, Petazzi E, Lanceni AG, Della Bosca E, Buttignol S, Starace A, Verusio C, Bortolato B. CBCT-based Prostate IGRT With and Without Implanted Markers: Assessment of Geometric Corrections and Time for Completion. Anticancer Res 2023;43:405-8.
30. Oultram S, Dempsey S. A Feasibility Study on the Identification of Postlumpectomy Seromas by a Radiation Therapist Compared with That by Radiation Oncologists in Radiation Therapy Planning for Early Stage Breast Cancer. J Med Imaging Radiat Sci 2018;49:173-8.
31. Topolnjak R, de Ruiter P, Remeijer P, van Vliet-Vroegindeweij C, Rasch C, Sonke JJ. Image-guided radiotherapy for breast cancer patients: surgical clips as surrogate for breast excision cavity. Int J Radiat Oncol Biol Phys 2011;81:e187-95.
32. Xiao A, Jutzy J, Hubert G, Edens M, Washington M, Hasan Y, Chmura SJ, Al-Hallaq HA. A study of the dosimetric impact of daily setup variations measured with cone-beam CT on three-dimensional conformal radiotherapy for early-stage breast cancer delivered in the prone position. J Appl Clin Med Phys 2020;21:146-54.
33. Zhang Y, Zhou H, Chu K, Wu C, Ge Y, Shan G, Zhou J, Cai J, Jin J, Sun W, Chen Y, Huang X. Setup error assessment based on "Sphere-Mask" Optical Positioning System: Results from a multicenter study. Front Oncol 2022;12:918296.
34. Chen Y, Zhang J, Ge Y, Zhang B, Chai L, Cai J, Yan J, Liu B. Accuracy and efficiency of an infrared based positioning and tracking system for image-guided intervention. 2016 IEEE 10th International Conference on Nano/Molecular Medicine and Engineering (NANOMED); 2016 Oct 30-Nov 02; Macau, China; IEEE, 2016.
35. Zhang J, Ge Y, Chen Y, Chen X. A study on the positioning accuracy of patient positioning based on Optical Positioning System for nasopharyngeal carcinoma: Compared with conventional method. 2013 IEEE International Conference on Medical Imaging Physics and Engineering; 19-20 October 2013; Shenyang, China; IEEE, 2013:11-3.
36. Grover S, Xu MJ, Yeager A, Rosman L, Groen RS, Chackungal S, Rodin D, Mangaali M, Nurkic S, Fernandes A, Lin LL, Thomas G, Tergas AI. A systematic review of radiotherapy capacity in low- and middle-income countries. Front Oncol 2015;4:380.
37. Zhang Y, Yi J, Jiang W, Liu J, Ma K, Kang S, Lang J, Wang J, Ren H, Li B, Zhang F, Lu B, Fu X, Chen M, Wang L. Survey on the Basic Information of Personnel and Facilities of Radiotherapy in Chinese Mainland in 2019. China Cancer 2020;29:321-6.
38. Mohandass P, Khanna D, Kumar TM, Thiyagaraj T, Saravanan C, Bhalla NK, Puri A. Study to Compare the Effect of Different Registration Methods on Patient Setup Uncertainties in Cone-beam Computed Tomography during Volumetric Modulated Arc Therapy for Breast Cancer Patients. J Med Phys 2018;43:207-13.
39. Batumalai V, Holloway L, Delaney GP. A review of setup error in supine breast radiotherapy using cone-beam computed tomography. Med Dosim 2016;41:225-9.
40. Velec M, Waldron JN, O'Sullivan B, Bayley A, Cummings B, Kim JJ, Ringash J, Breen SL, Lockwood GA, Dawson LA. Cone-beam CT assessment of interfraction and intrafraction setup error of two head-and-neck cancer thermoplastic masks. Int J Radiat Oncol Biol Phys 2010;76:949-55.
41. Liang J, Liu Q, Grills I, Guerrero T, Stevens C, Yan D. Using previously registered cone beam computerized tomography images to facilitate online computerized tomography to cone beam computerized tomography image registration in lung stereotactic body radiation therapy. J Appl Clin Med Phys 2022;23:e13549.
42. Hou J, Guerrero M, Chen W, D'Souza WD. Deformable planning CT to cone-beam CT image registration in head-and-neck cancer. Med Phys 2011;38:2088-94.
43. van Bunningen RH, Dijkstra PU, Dieters A, van der

Meer WJ, Kuijpers-Jagtman AM, Ren Y. Precision of orthodontic cephalometric measurements on ultra low dose-low dose CBCT reconstructed cephalograms. Clin Oral Investig 2022;26:1543-50.
44. Chen Y, Yin FF, Zhang Y, Zhang Y, Ren L. Low dose CBCT reconstruction via prior contour based total variation (PCTV) regularization: a feasibility study. Phys Med Biol 2018;63:085014.
45. Yuan N, Dyer B, Rao S, Chen Q, Benedict S, Shang L, Kang Y, Qi J, Rong Y. Convolutional neural network enhancement of fast-scan low-dose cone-beam CT images for head and neck radiotherapy. Phys Med Biol 2020;65:035003.
46. Cavedon C. Real-time control of respiratory motion: Beyond radiation therapy. Phys Med 2019;66:104-12.
47. Mulliez T, Gulyban A, Vercauteren T, van Greveling A, Speleers B, De Neve W, Veldeman L. Setup accuracy for prone and supine whole breast irradiation. Strahlenther Onkol 2016;192:254-9.
48. Ghaffari H, Navaser M, Mofid B, Mahdavi SR, Mohammadi R, Tavakol A. Fiducial markers in prostate cancer image-guided radiotherapy. Med J Islam Repub Iran 2019;33:15.
49. Pallotta S, Simontacchi G, Marrazzo L, Ceroti M, Paiar F, Biti G, Bucciolini M. Accuracy of a 3D laser camera surface imaging system for setup verification of the pelvic and thoracic regions in radiotherapy treatments. Med Phys 2013;40:011710.

Cite this article as: Zhang Y, Zhou H, Jiang Y, Wu C, Ge Y, Shan G, Chu K, Zhou J, Cai J, Jin J, Chen Y, Huang X. Improving the registration stability of cone-beam computed tomography with the Sphere-Mask Optical Positioning System: a feasibility study. Quant Imaging Med Surg 2023;13(5):2907-2921. doi: 10.21037/qims-22-989

